Seismic attenuation in a phase change coexistence loop

Yanick Ricard, J. Matas, F. Chambat

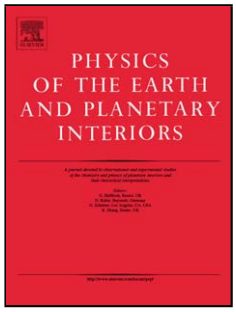

Title: Seismic attenuation in a phase change coexistence loop

Authors: Yanick Ricard, J. Matas, F. Chambat

PII: S0031-9201(09)00120-4
DOI: doi:10.1016/j.pepi.2009.04.007
Reference: PEPI 5167

To appear in: *Physics of the Earth and Planetary Interiors*

Received date: 26-11-2008
Revised date: 18-4-2009
Accepted date: 29-4-2009

Please cite this article as: Ricard, Y., Matas, J., Chambat, F., Seismic attenuation in a phase change coexistence loop, *Physics of the Earth and Planetary Interiors* (2008), doi:10.1016/j.pepi.2009.04.007

Seismic attenuation in a phase change coexistence loop

Yanick Ricard, J. Matas and F. Chambat
Laboratoire des Sciences de la Terre, CNRS, Université de Lyon, Bat Géode, 2 rue Raphael Dubois, 69622, Villeurbanne, 07, France.[1,1]

Abstract

Most phase transformations in the mantle occur across regions of multi-phase coexistence. Inside these regions, the long term incompressibility becomes very low because the density can increase both by compression and by changing phase. This difference between long term and elastic incompressibilities is a typical situation where seismic attenuation may happen. In this paper, we discuss the various differences between the classical theory of sound attenuation in a reacting fluid and the case of seismic propagation in a two-phase loop. We derive a simple analytical model of a two-phase loop to show that the phase change should affect both the bulk and the shear attenuation and in rather similar proportion. We show that attenuation occurs over two different frequency ranges. For the olivine-wadsleyite phase change, the low frequency attenuation occurs for periods larger than hundreds of years but the high frequency band occurs between 1 mn and 1 h (from 16 to 0.27 mHz) in the domain of surface waves and seismic modes. We predict both bulk and shear quality factors between 1-10 in the middle of the 410 km phase loop.

Key words: Seismic attenuation, phase change

The response to stress changes of the mineral aggregate that constitutes the mantle controls the velocity and dissipation of seismic waves. As it is generally easier to work with arrival times or velocities of seismic waves than with their amplitudes, the seismologists have made more remarkable progress in mapping radial or 3D velocity structures than in mapping the attenuation. The scattering of seismic waves by small scale heterogeneities and the focussing-defocussing effects of wave propagation in the presence of 3D velocity structures are indeed difficult to separate from intrinsic atten-

uation. In spite of observational difficulties, several global models of 1D attenuation have however been published (e.g. Dziewonski and Anderson, 1981; Widmer et al., 1991; Durek and Ekstrom, 1996). The disagreement between them is however large and often larger than the uncertainties suggested by each individual model (see e.g., Romanowicz and Mitchell, 2007, for a discussion). Three dimensional models are also available but are still a challenge and only the structures of the largest wavelengths have been mapped (Gung and Romanowicz, 2004). A better knowledge of attenuation is necessary to interpret the tomographic images and would however significantly improve our knowledge of mantle temperature (Anderson and Given, 1982; Karato and Karki, 2001; Matas and Bukowinski, 2007; Brodholt et al., 2007; Lekic et al., 2009).

In the last 40 years, (e.g., Jackson and Anderson, 1970; Anderson, 1976; Karato and Spetzler, 1990), various attenuation mechanisms have been discussed including those due to phase changes. The attenuation of sound in a media undergoing a phase change is indeed a classical example of irreversible process that leads to attenuation (de Groot and Mazur, 1984). Recently Li and Weidner (2008) have succeeded in the very difficult laboratory measurement of attenuation that takes place across the mantle transition zone, due to the presence of phase changes. Their paper assumes that the phase change attenuation is only related to compression, i.e., to what seismologists call the "bulk attenuation" (the quantity of energy lost during an oscillation of a pure isotropic compression). This attenuation is accounted for by the quality factor Q_κ on which seismologists have very little resolution. Seismologists tend to ascribe most of the attenuation to the "shear attenuation" accounted for by the quality factor Q_μ.

In the laboratory, the pressure changes used to drive the phase change are at the gigapascal level, while those due to seismic wave propagation are much smaller, typically of order 10^{-7} GPa (e.g., Aki and Richards, 2002). To rescale their observations, Li and Weidner (2008) propose a qualitative model of attenuation where the pressure perturbation δP associated with the seismic wave would drive the phase change at the interface between two grains by a distance $d \propto \delta P$ and this length should be compared to the time t necessary for cation diffusion, with $t \propto d^2$. Their model suggests therefore that the attenuation and the relaxation times are related to the amplitude of the seismic perturbation. This non-linearity would invalidate various assumptions of seismology,

like the principle of linear superposition or the ability to describe the wavefield observation of an instrument as a series of convolutions. It would imply that seismic waves from large earthquakes see a more attenuating mantle than those from small ones.

The model of Li and Weidner (2008) is based on general considerations that are explained in more details in Jackson (2007). However, Jackson (2007) warns us that "no attempt has been made to model the time-dependent stress at the phase boundary or the transformation kinetics, potentially strongly influenced by the rheology of the surrounding medium". This is what we do in this paper where we propose a micro-mechanical model of a coexistence loop. We show that dissipation occurs in two different time periods and that the resulting attenuations are independent of the seismic wave amplitudes. We confirm that phase change loops may be the zones of large attenuations. We show that they should affect rather similarly the compressibility and the shear modulus.

1. Reaction rates of phase changes

The mechanism of attenuation due to a phase change in the mantle (or in a fluid) is easy to understand (de Groot and Mazur, 1984). The changes of pressure due to a propagating sound wave affect differently the chemical potentials of the various coexisting phases and thus modify locally the thermodynamic equilibrium. This drives a mineralogical phase change, a possible source of dissipation. However, the theory of seismic attenuation in the mantle cannot be directly derived from that of sound attenuation in fluids because the physics differs by at least four aspects.

- First, the propagation of elastic waves is related to the rigidity μ (entirely for the S waves, and partly for the P waves) which is not considered for sound wave attenuation in fluids.

- Second, contrary to gases or fluids that are usually used in textbooks to illustrate thermodynamics, the thermodynamic equilibrium in complex solid aggregates is related to stresses, not to pressure. The pressure is not a continuous quantity across the grain interfaces. According to Shimizu (1997), a chemical potential

tensor should be defined on interfaces and the reaction rate should also depend on the crystal orientation. We assume here that the equilibrium on an interface only depends on the stresses normal to this interface σ_n which is a continuous variable (Paterson, 1973). In the absence of any viscoelastic stresses, the normal stress and the pressure can be identified and the usual thermodynamic rules are recovered.

- Third, the rheology of the mantle is not only simply elastic but viscoelastic. Deviatoric stresses can relax for times larger than the Maxwell time of the viscoelastic mantle, the ratio of viscosity to rigidity (see e.g., Ricard, 2007).

- Fourth, the phase transformations in the mantle are not univariant. As mantle materials are solid solutions and involves various cations, the phase changes occur across phase loops where two of more phases of various compositions coexist. For example, around 410 km, an olivine with a Fe/Mg ratio typically of 1/10 (Ringwood, 1982), enters a phase loop where wadsleyite, with a larger Fe/Mg ratio, nucleates and then grows. This larger ratio is balanced by a symmetrical decrease of the Fe/Mg ratio in the remaining olivine. Across the phase loop the percentage of wadsleyite increases with depth and this wadsleyite has a decreasing Fe/Mg ratio until the ratio of 1/10 which corresponds to the disappearance of the last grains of olivine. Notice that in a phase loop, the two phases are already present and the nucleation of new grains should not control the kinetics of transformation, contrary to what may happen when a single phase moves through a phase transition (Rubie and Ross, 1994).

The sound propagation theory shows that the attenuation is ultimately related to the difference between the elastic parameters at very high frequency (the unrelaxed parameters) and those at very low frequency (the relaxed parameters) if the relaxation occurs within the period of the sound wave. The time dependent pressure variations $\delta P(t)$ due a a high frequency seismic body wave, and the associated density variations $\delta\rho(t)$ are related by

$$\delta P(t) = \kappa_\infty \frac{\delta\rho(t)}{\rho}, \tag{1}$$

where κ_∞ is the elastic incompressibility (or elastic bulk modulus). The subscript ∞ indicates that this corresponds to the limit of infinite frequency, $\omega = +\infty$. More precisely, κ_∞ should be the isentropic incompressibility κ_S but we will not distinguish in this paper between the isothermal and isentropic elastic incompressibilities, κ_T and κ_S, that are at any rate, equal within 1%.

At thermodynamic equilibrium, inside a multi-phase loop where the density jumps by $\Delta\rho$ over a depth range ΔP, depth dependent pressure variations and depth dependent density variations are roughly proportional and related by

$$\frac{dP}{dr} = \frac{\kappa_0}{\rho}\frac{d\rho}{dr} \text{ with } \kappa_0 = \rho\frac{\Delta P}{\Delta\rho}. \quad (2)$$

The equilibrium relation (2) defines the relaxed bulk modulus in the limit of zero frequency.

If we take the example of the phase change around 410 km depth, between olivine and wadsleyite, the unrelaxed incompressibility (elastic bulk modulus) is around $\kappa_\infty = 180$ GPa. With an average density of 3630 kg m^{-3} and a density jump of 180 kg m^{-3} over a thickness of 10 km (this value is reasonable although estimates ranging from 5 to 30 km have been proposed (see e.g., Shearer, 2000; Van der Meijde et al., 2003; Ricard et al., 2005)), the relaxed incompressibility is $\kappa_0 = 7$ GPa. Outside a coexistence loop, the elastic incompressibility κ_∞ that can be measured by a time dependent phenomenon (the propagation of elastic waves) and the incompressibility measured along a radial profile κ_0 are usually considered as equal (or at least very close, see e.g., Bullen, 1940).

The numerical expression of κ_0 in eq. (2) can be expressed in a more physical way that demonstrates that κ_0 is bounded by κ_∞ (Li and Weidner, 2008). The density jump across a phase change $\Delta\rho$ is due both to an intrinsic density jump $\Delta\rho_\chi$ (the density difference between the two phases at a given pressure and temperature) and to the compression of the material across the coexistence loop. In other term, the relaxed compressibility in the phase loop, $1/\kappa_0$, is due both to the elastic compressibility $1/\kappa_\infty$ and to an apparent compressibility to the density jump $\Delta\rho_\chi$ existing between the two

phases so that

$$\frac{1}{\kappa_0} = \frac{1}{\kappa_\infty} + \frac{\Delta\rho_\chi}{\rho}\frac{1}{\Delta P} > \frac{1}{\kappa_\infty}. \tag{3}$$

When the transition thickness becomes very large, κ_∞ and κ_0 become therefore equal.

The evolution of an interface interacting with an elastic wave can be computed from the mechanical properties of the two phases and the boundary conditions on the interface. At the interface between grains, the total normal stress (pressure plus deviatoric stress) and shear stress are continuous. The boundary condition for the velocity across the reacting interface is expressed by

$$\rho_\alpha(\mathbf{v}_\alpha - \mathbf{V}).\mathbf{n} = \rho_\beta(\mathbf{v}_\beta - \mathbf{V}).\mathbf{n} = -\Delta\Gamma, \tag{4}$$

where ρ_i and v_i are the densities and the velocities of each phase, $\mathbf{n}$ the normal to the interface of the two media, directed from α to β, $\mathbf{V}$ the interface velocity and $\Delta\Gamma$ the reaction rate of the $\alpha \rightarrow \beta$ reaction (in kg m^{-2} s^{-1}). The velocity jump across the interface is therefore

$$(\mathbf{v}_\alpha - \mathbf{v}_\beta).\mathbf{n} = -\frac{\Delta\rho}{\rho_\alpha\rho_\beta}\Delta\Gamma, \tag{5}$$

where $\Delta\rho$ stands for $\rho_\beta - \rho_\alpha$.

Although the expression of the reaction rate $\Delta\Gamma$ might be very complex, it must cancel when the two phases are at thermodynamic equilibrium. The definition of the thermodynamic equilibrium is however subtle in the two-phase loop, and we discuss here two possible equilibrium conditions. We show in the following that the choice of one or the other expression does not change our conclusions on the seismic attenuation within the two-phase loop.

When the material inside a phase loop is at equilibrium, the reaction rate is zero. When the system is perturbed, for example by a change of the far-field pressure, the normal stress on interfaces changes. The rules of irreversible thermodynamics (de Groot and Mazur, 1984) suggests that the reaction rate close to equilibrium is proportional to the distance to equilibrium, i.e. to the change of affinity of the reaction.

The associated changes of chemical potentials are initially related to the normal stress perturbations on the grain interfaces $\delta\sigma_n$. Therefore the reaction rate has often

been chosen in previous modelling to be (e.g. Morris, 2002; Krien and Fleitout, 2008)

$$\Delta\Gamma \propto -\delta\sigma_n, \tag{6}$$

(the minus sign comes from the convention sign for normal stress, opposite to pressure, in fluid mechanics). For a very slow perturbation, however, the equation (6) cannot hold. On a time scale for which inter atomic diffusion occurs, the Fe/Mg content of each phase evolves, and as the chemical potentials are also functions of composition, a new equilibrium is found. The reaction occurs until the pressure change and the density change are related by the condition (2). This implies to choose

$$\Delta\Gamma \propto -\delta\sigma_n - \kappa_0 \frac{\delta\rho}{\rho}. \tag{7}$$

This relation could be rigourously obtained by following the more formal derivation of de Groot and Mazur (1984) provided the pressure replaces the normal stress. As κ_0 is very small, we will see that the difference in the attenuation predictions between using (6) or (7) is however only sensible at very long periods, outside the seismic frequency band.

We now need to define the geometrical distribution of the phases inside the loop and use (4) with (6) or (7) to be able to predict the effect of a seismic wave on the interface and thus on the attenuation. We assume that in each half of a phase loop, the minor phase is made of spherical grains surrounded by the major phase (Morris, 2002). For example, in the shallower half of the 410 km depth transition, we consider the β-phase as surrounded by the α matrix (see Figure 1). The outer radius R_e represents the average distance between the grains with radii $r \leq R_e$ of the minor phase. In the deepest part of the loop, the major β-phase is supposed to surround the last grains of α phase. This model will be used to describe the whole loop, although it is obvious that none of the two phases surrounds the other one in the middle of the loop.

When the normal stress on an interface is increased, a new film of the high pressure β-phase grows at the expense of the low pressure α-phase. This reaction, associated with minor changes of volume, facilitates the deformation, decreases the effective

strength, dissipates the elastic energy and therefore leads to attenuation. Notice that with the low pressure changes involved during the propagation of a seismic front, $\sim 10^{-7}$ GPa, the thickness of the reacting film is only nanometric (Li and Weidner, 2008). This very small perturbation is however a significant source of dissipation.

2. Radial deformation and complex incompressibility

We assume for simplicity that the two phases have the same elastic properties with bulk modulus κ and rigidity μ. We neglect the difference of these parameters for the two phases which is of the order of the jumps in incompressibility and rigidity, about 10% in PREM, at 410 km depth (Dziewonski and Anderson, 1981). We introduce the normalized radius $s = r/R_e$ where R_e is the external radius and we use S for the value of s on the two-phase interface.

In the case of isotropic radial compression of the two medium of Figure 1, it is straightforward to show that with spherical symmetry the radial deformation $u_r(s)$ in an elastic shell of compressibility κ_∞ and rigidity μ can be written

$$u_r^i = a_i s + \frac{b_i}{s^2}, \tag{8}$$

with $i = \alpha$ in the outer shell and $i = \beta$, inside (b_β is obviously 0 to insure that u_r^β is finite at $s = 0$). The change of density is

$$\delta\rho = -3\bar{\rho}\frac{u_r(R_e)}{R_e}, \tag{9}$$

and the effective compressibility of the medium is κ,

$$\kappa = \bar{\rho}\frac{\delta P}{\delta\rho} = -\frac{R_e}{3u_r(R_e)}\delta P, \tag{10}$$

where $u_r(R_e)$ and δP are the radial displacement and the pressure perturbation at the outer radius R_e.

By using the general expression of the jump of normal velocity (5) and one of the

kinetic laws (6) or (7), we can write

$$v_\alpha - v_\beta = C\left(\delta\sigma_n(S) - 3\kappa_0\frac{u(R_e)}{R_e}\right), \tag{11}$$

where C is a kinetic factor in m s^{-1} Pa^{-1} (the factor C includes the $\Delta\rho/\rho_\alpha\rho_\beta$ term of (5)). By choosing a vanishingly small κ_0 or the κ_0 deduced from the observed thickness of the transition we will be in agreement with (6) or with (7).

If a sinusoidal pressure perturbation of frequency ω, $\delta P\exp(i\omega t)$, is applied on the external rim, the deformations and therefore the coefficients a_i and b_i, will also vary at the same frequency. From the general expression of the deformation, (8), the normal stress can be expressed (see Appendix A). By matching the normal stresses across the phase boundary at s and using the normal velocity jump condition (11) with $v_\alpha = i\omega u_r^\alpha$ and $v_\beta = i\omega u_r^\beta$, the three constants a_α, b_α and a_β can be found from which the effective incompressibility (10) is readily obtained (see Appendix A).

We get

$$\kappa_{HF} = \kappa_\infty + \frac{\kappa_i - \kappa_\infty}{1 + i\omega\tau_1}, \tag{12}$$

(HF stands for "high frequency" as it will be explained below) where

$$\kappa_i = \kappa_\infty - S^3(\kappa_\infty - \kappa_0)\frac{\kappa_\infty + 4\mu_\infty/3}{\kappa_\infty S^3 + 4\mu_\infty/3}, \tag{13}$$

and where the relaxation constant τ_1 is

$$\tau_1 = \frac{R_e S}{3C\kappa_\infty}\frac{\kappa_\infty + 4\mu_\infty/3}{\kappa_\infty S^3 + 4\mu_\infty/3}. \tag{14}$$

The use of the subscripts i for "intermediate" will soon be explained. The incompressibility at infinite frequency which is usually called the unrelaxed incompressibility is simply the elastic incompressibility κ_∞, while κ_i is the relaxed incompressibility obtained for $\omega = 0$.

It might be surprising that the relaxed incompressibility κ_i in this model does not correspond to the incompressibility κ_0 (see (2)) obtained from a radial seismological model. This is because in a purely elastic model, the deviatoric stresses remain in the

elastic matrix even at infinite time. To clarify this point we have to remember that at large times, the Earth mantle does not behave as elastic but as viscous. The rigidity in the definition of κ_i, is in fact the high frequency limit of a viscoelastic rheology (see e.g., Ricard, 2007)

$$\mu^* = \mu_\infty \frac{i\omega\tau_M}{1+i\omega\tau_M}, \tag{15}$$

where τ_M is the Maxwell time, ratio of viscosity to rigidity (the real elastic rigidity). If we redo the same modeling using μ^* instead of μ_∞ we get the same expressions as (12) and (13) but where μ^* replaces μ_∞. The new expression of the viscoelastic incompressibility can be simplified and becomes after some algebra

$$\kappa = \kappa_\infty + \frac{\kappa_i - \kappa_\infty}{1+i\omega\tau_1} + \frac{\kappa_0 - \kappa_i}{(1+i\omega\tau_1)(1+i\omega\tau_2)}, \tag{16}$$

with the long relaxation time τ_2

$$\tau_2 = \tau_M \frac{\kappa S^3 + 4\mu/3}{\kappa S^3}. \tag{17}$$

We can safely assume, at least for the olivine-wadsleyite transformation (see e.g., Li and Weidner, 2008), that $\tau_1 << \tau_2 \sim \tau_M$, i.e., that the reaction occurs in a time shorter than the Maxwell time of a few hundred years. As is physically expected, the high frequency limit, when $1 << \omega\tau_1 << \omega\tau_2$ is the elastic value $\kappa = \kappa_\infty$ and the low frequency limit $\omega\tau_1 << \omega\tau_2 << 1$ is the incompressibility deduced from the thickness of the phase loop, $\kappa = \kappa_0$. The incompressibility variations occur within two frequency bands, one for $\omega\tau_1 \sim 1$ (and thus $\omega\tau_2 >> 1$) in which we recover (12),

$$\kappa \simeq \kappa_{HF} = \kappa_\infty + \frac{\kappa_i - \kappa_\infty}{1+i\omega\tau_1}, \tag{18}$$

where HF stands for high frequency and a second one for $\omega\tau_2 \sim 1$ (and $\omega\tau_1 << 1$) in which we get

$$\kappa \simeq \kappa_{LF} = \kappa_i + \frac{\kappa_0 - \kappa_i}{1+i\omega\tau_2}. \tag{19}$$

This is the low frequency approximation of κ. The low frequency limit of the high frequency incompressibility, $\omega = 0$ in (18), is κ_i which of course is also the high

frequency limit of the low frequency incompressibility, $\omega = +\infty$ in (19). In other words, the intermediate incompressibility κ_i that we considered as relaxed with respect to the short time scale of phase change can in turn be seen as unrelaxed with respect to the large time scale of viscous flow.

Using experiments of Kubo et al. (1998) on growth of wadsleyite from olivine at 13.5 GPa and 1300 K, Morris (2002) suggests that the kinetic constant is $C = 45$ nm s^{-1} GPa^{-1}. Although it is not obvious to derive a value of C from the paper of Li and Weidner (2008), they mention reaction lengths of a few μm, in $\sim$1 h, for pressure offsets of ~ 0.1 GPa which, within one order of magnitude, corresponds to the same range of kinetic constant. We choose a Maxwell time of $\tau_M = 174$ yr corresponding to a viscosity of 10^{21} Pa s, and a radius R_e corresponding to the average distance between grains equal to 1 mm.

We show in Figure 2 the evolution of the time constants τ_1 to τ_2 across the phase change. The volume ratio of β-phase across the loop varies more or less linearly with depth. The time constants are assumed symmetrical with respect to the vertical axis, $S^3 = 1/2$ (we assume that the minor phase is always in the inner sphere; the β-phase proportion is thus S^3 until a proportion of 50%, $1 - S^3$ after). They do not vary much across the phase transition except when a phase is in a very small proportion. The short time constants for incompressibility relaxation τ_1 is lower than 48 s. The long time constant τ_2 is larger than the Maxwell time τ_M.

Figure 3 depicts the evolution of the real and imaginary part of the incompressibility in the middle of the phase loop, $(S^3 = 1/2)$. The kinetic laws (6) and (7) have been used for the results of Re(κ) depicted with thick and thin lines, respectively. The two curves are very similar for short periods where the elastic incompressibility is recovered. They differ at long periods where the equilibrium in the loop imposes a relation between density and pressure given by the incompressibility κ_0. For intermediate periods, the phase change is inhibited by the elastic stresses controlled by the rigidity. The relaxation occurs in two steps over two different time ranges. During the high frequency relaxation, the reaction is limited by the elastic support that protects the minor phase. The reaction is controlled by diffusion and viscous relaxation at low frequency.

3. Pure shear deformation and complex rigidity

The existence of a phase change has also an effect on the rigidity. When at uniform pressure, the stresses are not uniform, the high pressure phase grows in the direction of the maximum stress and the reverse reaction occurs in the perpendicular direction. This eases the deformation and therefore reduces the effective rigidity. Notice that it is only because the chemical potential in solids is related to the normal stress not to the pressure (uniform in a pure shear deformation) than reactions occur.

An analytical expression can be obtained, although the derivation is more cumbersome and less rigourous than in the spherical case. Let us consider the deformation of a nucleus of β-phase surrounded by a shell of α-phase when a pure shear deformation is applied to the external boundary. The pure shear deformation far from the central nucleus is in cartesian coordinates $u_z = -\gamma z$, $u_x = \gamma x/2$ and $u_y = \gamma y/2$ (γ is the strain) and can be written in spherical coordinates after a standard change of coordinates

$$u_r = -\frac{1}{2}\gamma r(3\cos^2\theta - 1), \quad \text{and} \quad u_\theta = \frac{3}{2}\gamma r \cos\theta \sin\theta, \tag{20}$$

where θ is the colatitude.

In a pure shear experiment performed in a laboratory, the rigidity would be the ratio between the vertical stress applied on the surface of a core sample, at position z, and the vertical strain measured at the same position $-z\sigma_{zz}(z)/2u_z(z)$. In our analytical model, instead of imposing the deformation on surfaces of constant cartesian coordinates, they are imposed on the sphere or radius R_e. We consider that the effective rigidity can however be estimated by

$$\mu = -\frac{\sigma_{rr}(R_e,\theta))R_e}{2u_r(R_e,\theta)}. \tag{21}$$

We can solve for the deformation inside the two-phase aggregate by assuming that it keeps the same degree 2 geometry. As the radial stress and the radial deformation have the same geometry, μ is independent of θ. In this case, the general solution of the

momentum balance yields

$$u_r^i = \left(a_i s + b_i s^3 + \frac{c_i}{s^2} + \frac{d_i}{s^4} \right) (3\cos^2\theta - 1) \tag{22}$$

and

$$u_\theta^i = \left(-3a_i s - b_i \frac{7\mu + 5\lambda_\infty}{\lambda_\infty} s^3 - 6\frac{\mu_\infty}{3\lambda_\infty + 5\mu}\frac{c_i}{s^2} + 2\frac{d_i}{s^4} \right) \cos\theta \sin\theta \tag{23}$$

where s is again the normalized radius $s = r/R_e$, $\lambda_\infty = K_\infty - 2\mu_\infty/3$ is an elastic Lamé parameter, and i stands for α or β.

Using (22) and (23), the stress tensor can be computed in the inner sphere and in the outer shell (see Appendix B). The final resolution involves the determination of 6 parameters a_α, b_α, c_α, d_α, a_β and b_β. They can be obtained by matching 6 boundary conditions; the continuity of shear stress, normal stresses and tangential deformation on the interface, the jump condition for the normal velocity on the interface, and the 2 external boundary conditions (20) (see Appendix B). Notice that no density variation occurs in the assemblage submitted to a pure shear and the kinetic law (6) is therefore appropriate. Similarly to what we obtain for the incompressibility, the effective rigidity deduced from the model can be written as

$$\mu_{HF} = \mu_\infty + \frac{\mu_i - \mu_\infty}{1 + i\omega\tau_3}. \tag{24}$$

where the intermediate rigidity μ_i is

$$\mu_i = \mu_\infty - \mu_\infty F(S, \frac{\kappa_\infty}{\mu_\infty}), \tag{25}$$

where F is a cumbersome function of S and κ_∞/μ_∞. We can choose for simplicity $\kappa_\infty = 5\mu_\infty/3$ which corresponds to a Poisson ratio of 1/4 (or to the equality of the two Lamé Parameters λ_∞ and μ_∞, (e.g. Malvern, 1969)) which is a common rule of thumb for elasticity of silicates. In this case, the function F is

$$F(S, \frac{\kappa_\infty}{\mu_\infty} = \frac{5}{3}) = 105S^3 \frac{8 + S^2}{604 + 280S^3 + 56S^5 + 5S^7}, \tag{26}$$

and the relaxation times τ_3 is

$$\tau_3 = 315\frac{SR_e}{C\mu_\infty}\frac{1}{604 + 280S^3 + 56S^5 + 5S^7}. \quad (27)$$

The constant τ_3 of shear modulus relaxation is also depicted in Figure 2 and its value is comparable to that appearing in the high frequency incompressibility τ_2.

Like for the incompressibility, the intermediate rigidity μ_i that corresponds to the relaxed limit of the rigidity with respect to the short time scale of phase change can in turn be seen as an unrelaxed rigidity for periods larger than τ_3 but much smaller than the Maxwell time. Replacing directly in (24) and (25), μ_∞ by μ^*, see (15), is straightforward but leads to a very complex expression of μ. We checked numerically that the behavior of $\mu^* F(\kappa_\infty/\mu^*)$ can be qualitatively approximated by $\mu^* F(\kappa_\infty/\mu_\infty)$. For periods much larger than τ_3, the rigidity varies therefore as

$$\mu = \left(\mu_\infty + \frac{\mu_i - \mu_\infty}{1 + i\omega\tau_3}\right)\frac{i\omega\tau_M}{1 + i\omega\tau_M}. \quad (28)$$

As $\tau_3 << \tau_M$, the expression of the rigidity at high frequency, when $\omega\tau_M >> 1$ is $\mu \simeq \mu_{HF}$. At low frequency, when $\omega\tau_3 << 1$ we get

$$\mu \simeq \mu_{LF} = \mu_i - \frac{\mu_i}{1 + i\omega\tau_M}, \quad (29)$$

which reaches zero after complete relaxation when $\omega = 0$, i.e., when the medium behaves viscously rather than elastically.

The real and imaginary parts of the rigidity are plotted in Figure 3. Like for the incompressibility, two transitions are predicted. The low frequency transition only occurs when the elastic stresses in the surrounding shell relax and stop screening the inner nucleus from the outside stresses. At zero frequency (infinite period), the rigidity vanishes contrary to the incompressibility that remains finite.

4. Bulk and shear attenuations

In the case of complex elastic parameters, the seismic waves propagates with a frequency-dependent attenuation usually defined by the quality factors Q_ξ where ξ stands for κ or μ. These quality factors are defined by

$$Q_\xi = -\frac{\mathrm{Re}(\xi)}{\mathrm{Im}(\xi)} = \frac{\xi^R + \xi^U \omega^2 T_R^2}{(\xi^U - \xi^R)\omega T_R}, \tag{30}$$

where T_R is the appropriate relaxation time, $\mathrm{Re}(\xi)$ and $\mathrm{Im}(\xi)$ the real and imaginary parts of ξ that varies between the relaxed and unrelaxed limits, ξ^R (for $\omega = 0$) and ξ^U (for $\omega = +\infty$). Attenuation is maximum at the frequency

$$\omega_0 = \frac{1}{T_R}\sqrt{\frac{\xi^R}{\xi^U}}, \tag{31}$$

where Q_ξ reaches its minimum

$$Q_\xi^0 = 2\frac{\sqrt{\xi^R \xi^U}}{\xi^U - \xi^R}. \tag{32}$$

Notice that in our model, each elastic parameter has low and high frequency modes. The bulk modulus can relax from $\xi^U = \kappa$ to $\xi^R = \kappa_i$ with the time constant τ_1, then from $\xi^U = \kappa_i$ to $\xi^R = \kappa_0$ with the time constant τ_2. Similarly, the rigidity relaxes from $\xi^U = \mu$ to $\xi^R = \mu_i$ with the time constant τ_3, then from $\xi^U = \mu_i$ to $\xi^R = 0$ with the time constant τ_M.

Figure 5 depicts the minimum quality factor Q_κ^0 and Q_μ^0 for the various relaxation times and across the two-phase loop. Like for Figure 2, we assume that our model is valid until $S^3 = 1/2$, then swap the roles of the minor and major phases, which simply symetrises the results with respect to the middle of the loop. Values lower than 10 are predicted for the high frequency bands. The bulk attenuation in the coexistence loop observed by Li and Weidner (2008) is indeed found maximum when the two phases are in similar proportions, as predicted by our model. To compute the bulk attenuation, we use either a κ_0 deduced from the thickness of the phase change (thick line, see eq. (7)) or $\kappa_0 = 0$ (thin line, see (6)). This does not really change the predicted quality

factor. The low frequency bulk attenuation is very low but corresponds to very long time constants not relevant to seismology as seen on Figure 6.

Figure 6 depicts the attenuation quality factor Q_κ and Q_μ computed at the center of the phase loop ($S^3 = 1/2$) as a function of the period of the excitation. The solid lines correspond to the bulk attenuation, the dashed line to the shear attenuation. A minimum of quality factors is predicted for frequencies between 0.27 and 16 mHz (periods between 1 mn and 1 h). At very low frequencies, when the mantle behaves viscously, the quality factors become also very low. Assuming a zero κ_0 or a finite κ_0 is only visible at very long periods: the phase loop maintains a finite compressibility (thick line) in the latter case, but cannot resist compression (thin line) in the former case. The shear quality factor reaches zero at zero frequency where the mantle behaves viscously rather than elastically. The general behavior for the shear attenuation is that of a linear solid called a Burger body (see e.g. Karato and Spetzler, 1990). The bulk attenuation behaves differently as contrary to the Burger body, the quality factor does vanish at infinite periods.

The fact that the bulk quality factor is lower than the shear quality factor is not a general result of our model. The difference $\kappa_i - \kappa_\infty$ that controls the bulk attenuation is proportional to $\kappa_0 - \kappa_\infty$ (see (12) and (13)). This difference tend to decrease when the loop thickness increases (see (3)). On the contrary the difference $\mu_i - \mu_\infty$ controlling the shear attenuation is independent of the loop thickness (see (24)). The ratio $Q_\kappa/Q\mu$ decreases therefore with the loop thickness. Increasing the loop thickness over 50 km for the 410 km transition (keeping the other parameters unchanged) would lead to Q_μ lower than Q_κ. In other words, a thin loop is mostly attenuating because of its Q_κ, a thick one because of its Q_μ.

5. Conclusions

Our model of attenuation in coexistence loop is certainly simplified in particular in the description of the geometry of the two phases. However we believe that various aspects of our model are very robust.

We confirm that the phase loops, in agreement with Li and Weidner (2008) should

be the location of a significant attenuation for periods belonging to the low frequency seismic band (surface waves and seismic modes). However in their paper, only the bulk attenuation was taken into account whereas we have shown that the shear attenuation should be affected as well. Moreover, we found that the two attenuations and their relaxation times are independent of the amplitude of the seismic wave in agreement with the usual assumption of seismology. The attenuation bands are narrow because of our assumption of a unique grainsize across the coexistence loop. A distribution of grainsizes would probably broaden the frequency bands of attenuation.

Another large difference between Li and Weidner (2008) and the present paper is that the transition between the elastic incompressibility, κ_∞ and that deduced from PREM κ_0 (very low incompressibility in coexistence loops) does not occur in a single step but in two steps. This is summarized in Figure 7 where we plot as a function of depth the instantaneous κ_∞, the intermediate κ_i and the κ_0 bulk moduli. We derived a $\kappa_\infty(r)$ that follows the PREM values outside the loop and varies linearly within the loop. We introduce the same $\kappa_\infty(r)$ in the computation of κ_i, (13). These depth-dependent incompressibilities look more realistic, but truly our model assumes the κ_∞ is uniform within the loop. We predict that the transformation is first limited by the shielding of the external stresses by the elastic rigidity of the matrix. This behavior is in agreement with Morris (2002). This first "fast" transition between κ_∞ and κ_i (see Figure 7) occurs within minutes or hours. Therefore the incompressibility seen by seismology is somewhere between these two values. The final transformation (slow kinetics) corresponding to the transition between κ_i and κ_0 occurs in a second step when the elastic stresses are released, and a new two-phase equilibrium is found after diffusion and reequilibration of the composition. A very similar figure could be drawn for the rigidity, but the totally relaxed rigidity would simply be zero.

The minimum values of Q_κ and Q_μ predicted for the olivine-wadsleyite loop are significantly lower than the typical range of attenuation of low frequency seismologic models. This is true for the shear attenuation and even more for the bulk attenuation. In a recent review, Resovsky et al. (2005) propose for depths around 400 km a Q_μ roughly between 150 and 200 and Q_κ larger than 2000. These radial models have used a very simple parametrization of the attenuation in a limited range of layers (typically

larger than 200 km) and in layers than coincide with the seismic discontinuities. This parametrization is certainly an inappropriate choice to detect a narrow depth range of attenuation astride a velocity discontinuity.

The Q_κ and Q_μ quality factors seen by given seismic or tidal perturbations are not necessary the minimum values shown in Figures 5 or 6, but are functions of their frequencies, of the kinetic constant C and of the grain size R_e. The exact frequency dependent expressions for incompressibility, rigidity and attenuation can be easily computed from (12), (24) and (30). The values of C and R_e are still uncertain for the olivine-wadsleyite phase change and mostly unknown for other mantle phase changes. The narrow depth range of the coexistence loop, $\sim$ 10 km, may make this localized attenuation difficult to detect but may significantly bias the average determined over a large zone of sensibility. The presence of bulk attenuation in the upper mantle has indeed be proposed by various studies (Resovsky et al., 2005; Durek and Ekstrom, 1996).

The existence of a strong attenuation associated with seismic velocity jumps should also affect the reflection and transmission factors of short period seismic waves hitting these interfaces. Notice however that body waves seem to have a too high frequency to be right on the attenuation maximum, but according to Figure 6 might see an attenuation of order 10-100 (for frequencies between 1 Hz to 20 mHz). This could possibly be seen from S waves multiply reflected under the Earth surface and with a turning point below or above the 410 km discontinuity. At any rate, a better estimate of attenuation in phase loops would constrain the kinetic behavior of these phase changes (Chambat et al., 2009).

We have discussed the attenuation due to the olivine-wadsleyite transition because this transition is simple and only involves two phases of similar composition. Other mantle transitions should behave similarly like the wadsleyite-ringwoodite loop around 520 km deep (but, of course, with their appropriate kinetic laws that may not lead to characteristic times for the phase changes in tune with the seismic periods). The mantle transitions involving three phase like the ringwoodite to ferropericlase+perovskite, should also lead to attenuation because of a large difference between the relaxed and unrelaxed properties. However because of the necessary long distance motion of

atoms during the transformation, a model of kinetics seems yet difficult to propose.

Appendix A. Radial deformation

The deformation given by (8) corresponds to the radial stress

$$\sigma_{rr}^{i} = 3\kappa\frac{a_i}{R_e} - 4\mu\frac{b_i}{R_e s^3}. \tag{A-1}$$

The continuity of normal stress across the phase transition boundary satisfies

$$3\kappa a_\alpha - 4\mu b_\alpha \frac{1}{s^3} = 3\kappa a_\beta, \tag{A-2}$$

while the application of an external pressure corresponds to

$$3\kappa\frac{a_\alpha}{R_e} - 4\mu\frac{b_\alpha}{R_e} = -\delta P. \tag{A-3}$$

The condition of jump of normal displacement where the phase change occurs is

$$i\omega(a_\alpha s + \frac{b_\alpha}{s^2} - a_\beta s) = C(3\kappa\frac{a_\beta}{R_e} + \frac{\kappa_0}{\kappa_v}\delta P), . \tag{A-4}$$

The resolution of equations (A-2)-(A-4) leads to the unknowns a_α, b_α and a_β and therefore to the expression of the effective incompressibility (see (10))

$$\kappa = -\frac{R_e}{3(a_\alpha + b_\alpha)}\delta P. \tag{A-5}$$

Appendix B. Pure shear deformation

From expressions (22)-(23), stresses can then be readily obtained,

$$\sigma_{rr}^{i} = \frac{\mu}{R_e}(2a_i - b_i s^2 - 2\frac{9\lambda_\infty + 10\mu_\infty}{3\lambda_\infty + 5\mu_\infty}\frac{c_i}{s^3} - 8\frac{d_i}{s^5})(3\cos^2\theta - 1), \tag{B-1}$$

$$\sigma_{r\theta}^{i} = -2\frac{\mu}{R_e}(3a_i + \frac{8\lambda_\infty + 7\mu_\infty}{\lambda_\infty}b_i s^2 + 3\frac{3\lambda_\infty + 2\mu_\infty}{3\lambda_\infty + 5\mu_\infty}\frac{c_i}{s^3} + 8\frac{d_i}{s^5})\cos\theta\sin\theta, \tag{B-2}$$

where i stands for α or β.

To avoid unnecessary complexities, we assume $\lambda_\infty = \mu_\infty$ or $\kappa_\infty = 5\mu_\infty/3$. This time, the boundary conditions on the outer shell imply

$$a_\alpha + b_\alpha + c_\alpha + d_\alpha = -\frac{\gamma}{2}, \tag{B-3}$$

$$\frac{1}{4}(-12a_\alpha - 48b_\alpha - 3c_\alpha + 8d_\alpha) = \frac{3\gamma}{2}, \tag{B-4}$$

the continuity of radial and shear stress at the phase-change interface implies

$$(8a_\alpha - 4b_\alpha s^2 - 19\frac{c_\alpha}{s^3} - 32\frac{d_\alpha}{s^5}) = (8a_\beta - 4b_\beta s^2), \tag{B-5}$$

$$-(24a_\alpha + 120b_\alpha s^2 + 15\frac{c_\alpha}{s^3} + 64\frac{d_\alpha}{s^5}) = -(24a_\beta + 120b_\beta s^2), \tag{B-6}$$

and the continuity of θ-displacement

$$\frac{1}{4}(-12a_\alpha s - 48b_\alpha s^3 - 3\frac{c_\alpha}{s^2} + 8\frac{d_\alpha}{s^4}) = \frac{1}{4}(-12a_\beta s - 48b_\beta s^3). \tag{B-7}$$

As there is no global volume change in this pure shear experiment the jump of radial displacement is given by (6)

$$i\omega\left((a_\alpha s + b_\alpha s^3 + \frac{c_\alpha}{s^2} + \frac{d_\alpha}{s^4}) - (a_\beta s + b_\beta s^3)\right) = C\frac{1}{4}\frac{\mu_\infty}{R_e}(8a_\beta - 4b_\beta s^2). \tag{B-8}$$

The resolution of equations (B-3)-(B-8) leads to the unknowns a_α, b_α, c_α, d_α, a_β and b_β. At last, we estimate the effective shear modulus according to (21)

$$\mu = \frac{\mu_\infty}{4}\frac{8a_\alpha - 4b_\alpha - 19c_\alpha - 32d_\alpha}{a_\alpha + b_\alpha + c_\alpha + d_\alpha} \tag{B-9}$$

Acknowledgments

This work has been supported by the CNRS-INSU Dyeti program. We thank Tine Thomas for interesting discussions on seismic attenuation.

References

Aki, K., Richards, P. G., 2002. Quantitative seismology. University Science Books, New York.

Anderson, D. L., 1976. The earth as a seismic absorption band. Science 196, 1104–1106.

Anderson, D. L., Given, J. W., 1982. Absorption-band q model for the earth. J. Geophysical Research 87, 3893–3904.

Brodholt, J. P., Hellfrich, G., Trampert, J., 2007. Chemical versus thermal heterogeneity in the lower mantle: The most likely role of anelasticity. Earth Planetary Science Lett. 262, 429–437.

Bullen, K. E., 1940. The problem of the earth's density variation. Seismol. Soc. Am. Bull. 30, 235–250.

Chambat, F., Durand, S., Matas, J., Ricard, Y., 2009. Constraining the kinetics of mantle phase changes with seismic mode data. Earth Planetary Science Lett. in prep.

de Groot, S. R., Mazur, P., 1984. Non-Equilibrium Thermodynamics. Dover Publications, New York.

Durek, J., Ekstrom, G., 1996. A radial model of anelasticity consistent with long-period surface wave data. Bull. Seismol. Soc. Am. 86, 144–158.

Dziewonski, A. M., Anderson, D., 1981. Preliminary reference earth model. Phys. Earth. Planet. Inter.25, 297–356.

Gung, Y., Romanowicz, B., 2004. Q tomography of the upper mantle using three-component long-period waveforms. Geophysical J. Int. 157, 813–830.

Jackson, D. D., Anderson, D. L., 1970. Physical mechanisms of seismic-wave attenuation. Reviews of Geophys. and Space Phys. 8, 1–63.

Jackson, I., 2007. Physical origins of anelasticity and attenuation in rock. In: Schubert, G. (Ed.), Treatise of Geophysics. Vol. 2 Mineral Physics: Properties of Rocks and Minerals. Elsevier Scientific Publishing Company, New York, Ch. 2.17, pp. 496–522.

Karato, S., Spetzler, H. A., 1990. Defect microdynamics in minerals and solid-state mechanisms of seismic-wave attenuation and velocity dispersion in the mantle. Rev. Geophys. 28, 399–421.

Karato, S. I., Karki, B. B., 2001. Origin of lateral variation of seismic wave velocities and density in the deep mantle. J. Geophysical Research 106, 21771–21783.

Krien, Y., Fleitout, L., 2008. The accomodation of volume changes in phase transition zones: implications for mantle dynamics and metamorphism. J. Geophys. Res.

Kubo, T., Ohtani, E., Shinmei, T., Fujino, K., 1998. Effects of water on the $\alpha - \beta$ transformation kinetics in san carlos olivine. Science 281, 85–87.

Lekic, V., Matas, J., Panning, M., Romanowicz, B., 2009. Frequency dependence of shear wave attenuation. Earth Planetary Science Lett. in press.

Li, L., Weidner, D. J., 2008. Effect of phase transitions on compressional-wave velocities in the earth's mantle. Nature 454, 984–986.

Malvern, L., 1969. Introduction to the mechanics of a continuum medium. Prentice-Hall Series in Engineering of the Physical Sciences.

Matas, J., Bukowinski, M. S. T., 2007. On the anelastic contribution to the temperature dependence of lower mantle seismic velocities. Earth Planetary Science Lett. 259, 51–65.

Morris, S. J. S., 2002. Coupling of interface kinetics and transformation-induced strain during pressure-induced solid-solid phase changes. J. Mech. Phys. Solids 50, 1363–1395.

Paterson, M. S., 1973. Non hydrostatic thermodynamics and its geological applications. Rev. Geophys. 11, 355–389.

564 Resovsky, J., Trampert, J., van der Hilst, R. D., 2005. Error bars for the global q profile.
565 Earth Planetary Science Lett. 230, 413–423.

566 Ricard, Y., 2007. Physics of mantle convection. In: Schubert, G. (Ed.), Treatise of
567 Geophysics. Vol. 7 Mantle Dynamics of Treatise on Geophysics. Elsevier Scientific
568 Publishing Company, New York, Ch. 7.02, pp. 31–87.

569 Ricard, Y., Mattern, E., Matas, J., 2005. Mineral physics in thermod-chemical mantle
570 models. In: Composition, Structure and Evolution of the Earth Mantle. Vol. AGU
571 monograph 160. eds R. Hilst et al., pp. 283–300.

572 Ringwood, A., 1982. Phase transformations and differentiation in subducted litho-
573 sphere: implications for mantle dynamics, basalt petrogenesis, and crustal evolution.
574 J. Geol. 90 (6), 611–642.

575 Romanowicz, B., Mitchell, B., 2007. Q in the earth from crust to core. In: Schubert,
576 G. (Ed.), Treatise of Geophysics. Vol. 1 Seismology and Structure of the Earth of
577 Treatise on Geophysics. Elsevier Scientific Publishing Company, New York, Ch.
578 1.21, pp. 731–774.

579 Rubie, D., Ross, C. R., 1994. Kinetics of the olivine-spinel transformation in subduct-
580 ing lithosphere: experimental constraints and implications for deep slab processes.
581 Phys. Earth Planetary Interiors 86, 223–241.

582 Shearer, P. M., 2000. Upper mantle seismic discontinuities. In: Earth's Deep Interior:
583 mineral physics and tomography from the atomic to the global scale. Vol. AGU
584 monograph 117. eds S. Karato et al., pp. 115–131.

585 Shimizu, I., 1997. The non-equilibrium thermodynamics of intracrystalline diffusion
586 under non-hydrostatic stress. Philosophical Magazine A 75, 1221–1235.

587 Van der Meijde, M., Marone, M., Giardini, D., van der Lee, S., 2003. Seismic ev-
588 idence for water deep in earth's upper mantle. Science 300 (doi: 10.1126/sci-
589 ence.1083636.).

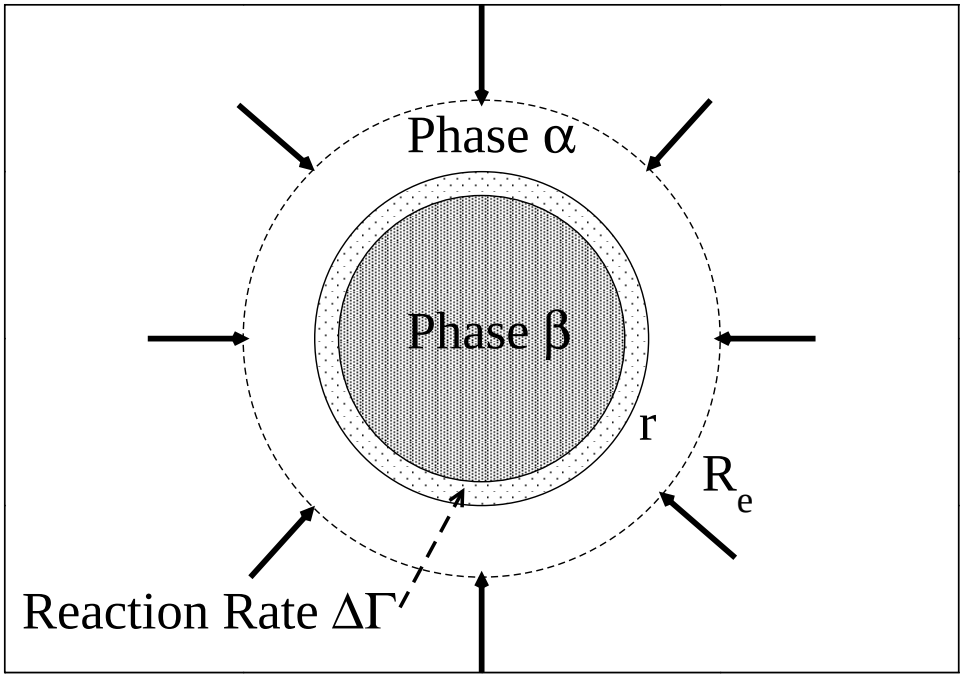

Figure 1: The growing β-phase is surrounded by the low pressure α-phase. The interface at radius r moves up or down depending of the applied external pressure that controls the reaction rate $\Delta\Gamma$. The external diameter $2R_e$ will be interpreted as the average distance between grains.

590 Widmer, R., Masters, G., Gilbert, F., 1991. Spherically symmetric attenuation within
591 the earth from normal mode data. Geophysical J. Int. 104, 541–553.

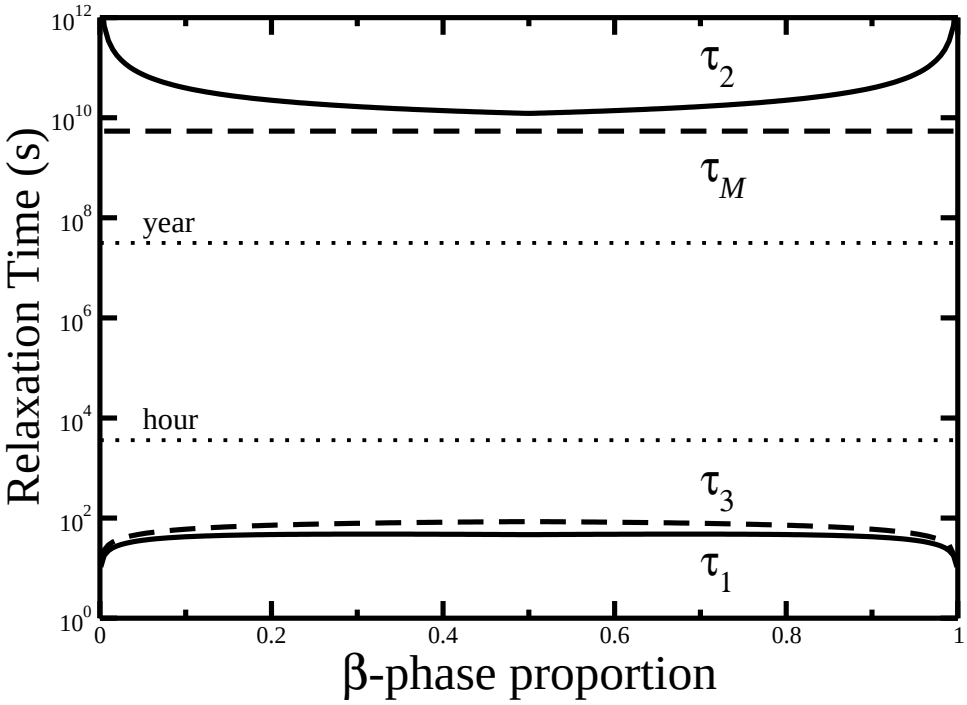

Figure 2: Relaxation times of incompressibility (τ_1 and τ_2) and shear modulus (τ_3 and Maxwell time τ_M) across a phase loop. The two short relaxation times are in the seismic band of surface waves, for the bulk attenuation τ_1 and the shear attenuation τ_3. The long bulk and shear relaxation times τ_2 and τ_M correspond to viscoelastic behaviours occurring after at least one Maxwell time. The horizontal lines correspond to periods of 1 h and 1 yr (frequencies of 0.27 mHz and 0.03 μHz).

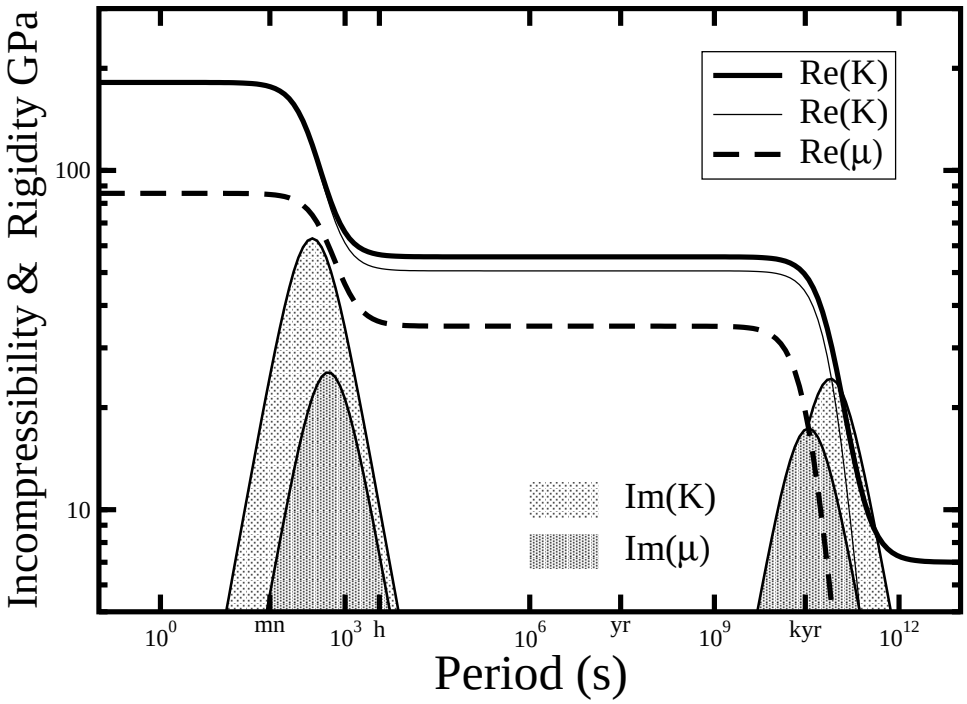

Figure 3: Incompressibility and rigidity as functions of the period. The real part is depicted by lines, the imaginary part by shadows. The thin line corresponds to the incompressibility computed using (6), the thick line using (7). In the former case the incompressibility goes to zero at long period while in the latter, it reaches the relaxed compressibility κ_0. The high frequency relaxation occurs for seismic and tidal periods.

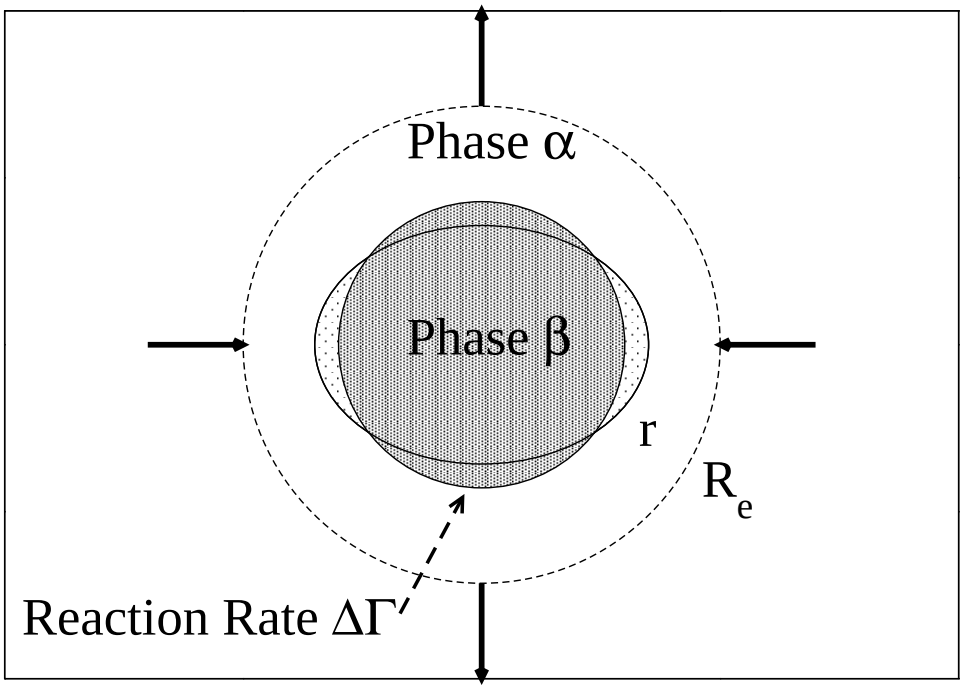

Figure 4: To compute the shear attenuation, we submit the two-phase to a pure shear experiment. The pressure remains constant, but the high pressure β-phase starts growing in the direction of the maximum stress, the α-phase in the direction of the lowest stress as the reaction rate is related to the normal stress on interfaces.

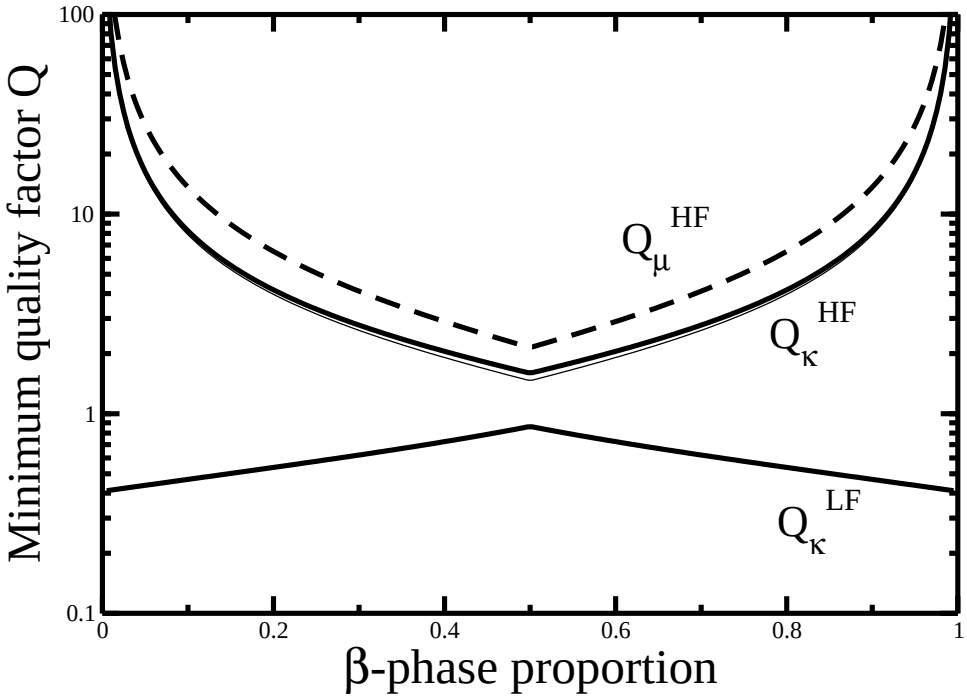

Figure 5: Evolution of the quality factor across the phase change. The volume proportion of the high pressure phase varies more or less linearly with depth with across the phase change. The high frequency quality factor for both Q_κ^0 and Q_μ^0 are below 10 in the center of the loop. The exact value of κ_0 (7 10^9 GPa, thick solid line, or 0, thin solid line) is not very important. The very low quality factor of Q_κ^0 at low frequency does not belong to the seismic or tidal domain.

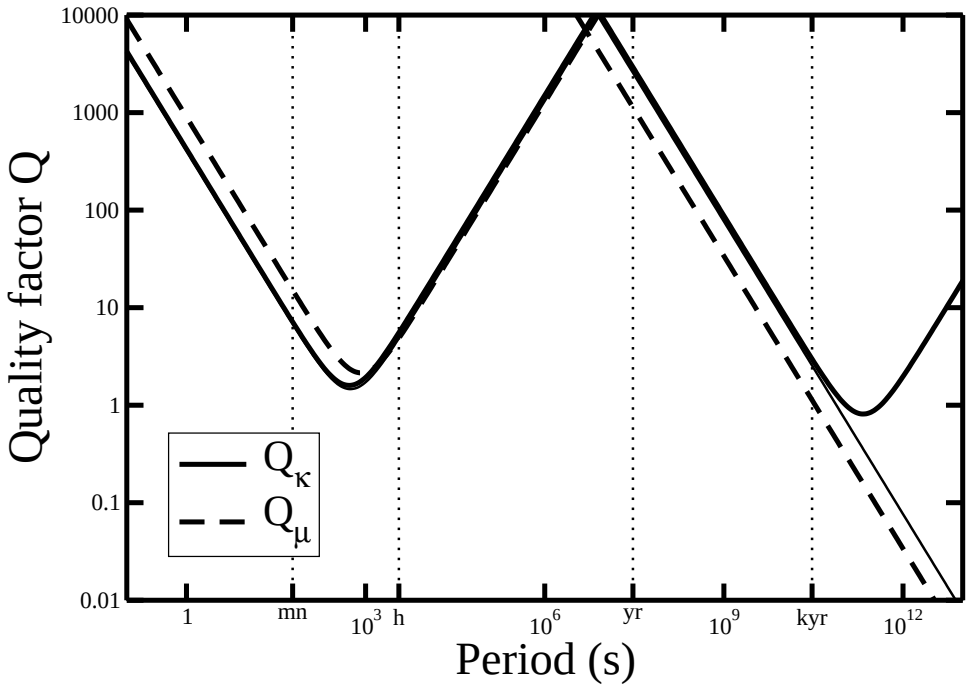

Figure 6: Quality factors at the middle of the phase loop, as a function of the period of the exitation. Two attenuation bands are predicted, one between 1 mn and 1 h (from 16 to 0.27 mHz) the other for times larger than the Maxwell time. The minima correspond to the extrema depicted at the middle of the phase loop in Figure 5. The thin line corresponds to the value of Q_κ computed with $\kappa_0 = 0$.

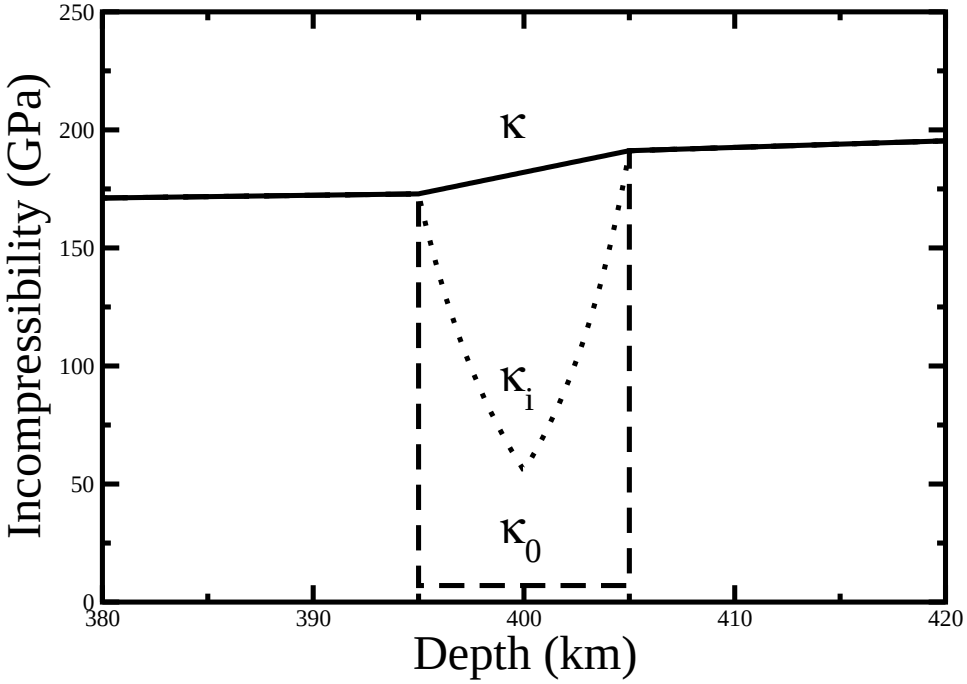

Figure 7: Various incompressibilities have been defined in this paper within a two-phase coexisting zone. The elastic incompressibility κ, seen by high frequency body waves, the totally relaxed compressibility κ_0 that can be deduced from the density jump and the thickness of the transition, and an intermediate incompressibility κ_i, see equation (13). The transition between κ and κ_i and an associated attenuation should occur for periods corresponding to surface waves. The transition between κ_i and κ_0 should take a much longer time (a Maxwell time larger than 100 yrs).